FATIGUE CRACK PROPAGATION UNDER TORSIONAL SPECTRUM LOAD OF A HELICOPTER TAIL ROTOR SHAFT AFTER BALLISTIC DAMAGE

A. Manes[1], L. Giudici[2], and M. Giglio[3]

[1] Politecnico di Milano, Dipartimento di Meccanica
Via La Masa 1 - 20156 Milano (Italy), Email: andrea.manes@polimi.it
[2] Politecnico di Milano, Dipartimento di Meccanica
Via La Masa 1 - 20156 Milano (Italy), Email: lorenzo.giudici@inwind.it
[3] Politecnico di Milano, Dipartimento di Meccanica
Via La Masa 1 - 20156 Milano (Italy), Email: marco.giglio@polimi.it

ABSTRACT
Experimental tests of impact of a 7.62 NATO projectile perforating a helicopter tail rotor shaft are briefly presented. Subsequently the damaged specimen has been tested with a multiaxial testing machine, in order to evaluate its capability to sustain a recovery mission, simulated by applying a torsional fatigue spectrum. During the test the nucleation and propagation of fatigue cracks have been monitored.
Finite Element analyses have been carried out to simulate both impact and crack propagation for a further analytical automated simulation of these conditions. According to the multiaxial state of stress induced by torque, residual stress field and shape of the damage, mixed mode propagation has been considered, by means of an equivalent SIF. Numerical results are in good agreement with experimental data.

Keywords: ballistic impact, tail rotor shaft, residual strength, experimental, numerical.

INTRODUCTION AND EXPERIMENTAL TESTS OF BALLISTIC IMPACT

According to the low altitude profile mission of military helicopters, a ballistic damage can occur and then the residual life assessment of critical components is fundamental. In this scenario the tail rotor transmission line is very exposed to such type of damage and in particular the shaft. In this work a thin-walled cylindrical tube made of 6061 T6 aluminium alloy equipped with two welded mounting flanges has been considered. This component is not a real tail rotor shaft of helicopter but simulates very well its features in terms of shape, material and dimensions. A common 7.62 NATO bullet has been chosen for the tests. In the determination of the worst damage condition, the offset and impact angle of the projectile, represented in Figure 1, play a primary role.
The angle of impact is defined as the angle between the trajectory of the projectile and the line normal to the generatrix of the tube (parallel to the longitudinal axis) in the impact point, where all the three objects (line, generatrix and trajectory) lie in the same plane. Instead the offset is the distance between the axis of the target and the trajectory

of the projectile. Based on several numerical simulations, object of previous studies [1], the theoretical worst condition, in terms of damage, has been identified for a shaft subjected to a torsion load. This critical condition, represented by impact angle of 45 ° and projectile surface tangent to the shaft surface, generates a single hole almost elliptical in shape, with axis tilted at 45° and maximum size. The simulations, conducted varying the offset of the projectile, have shown that decreasing the offset below the critical value, two separate holes for entry and exit of the projectile appear. On the contrary, increasing the offset beyond its critical value, a single hole or sometimes the "ricochet effect" of the projectile occur.

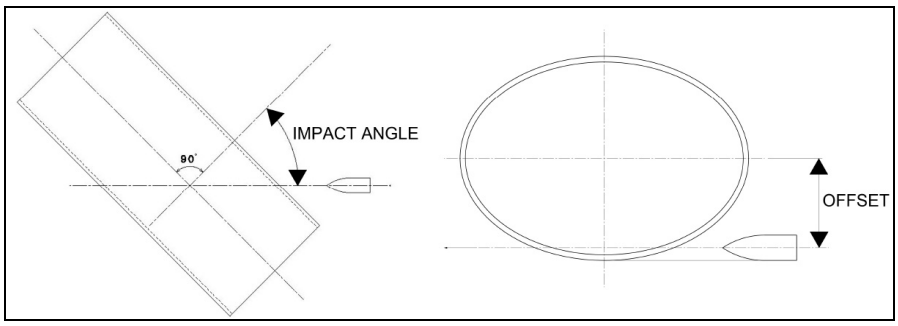

Figure 1 – Impact parameters.

The ballistic tests have been performed inside a dedicated shooting range equipped with gun, bullets, pointing system and laser/detectors to measuring the initial velocity of the projectile. Other equipments necessary to carry out the tests have been designed by the authors. Figure 2 shows the entire experimental set-up. A dedicated test rig has been built to support the shafts in the correct position (angle and offset). No instrumentation has been directly available to measure the residual velocity of the projectile after the perforation of the target, due to the risks of damage.

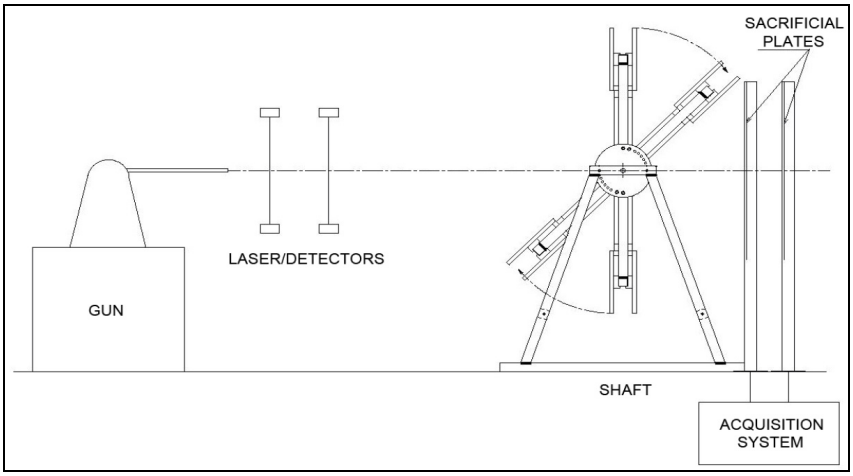

Figure 2 – Experimental set-up of the impact tests

Thus analyzing the methods used in other experimental investigations for this purpose [2-12], a semi-original system has been designed, based on the use of two accelerometers applied on two thin aluminium sheets: the perforation of the sheets generates two separate signals whose time interval of emission is detected by a dedicated acquisition system; then, knowing the distance between the plates it's easy to calculate the velocity of the projectile. Correction to consider kinetic energy dissipated during the perforation [13] and the delay due to the real trajectory of the projectile have been also considered.
A picture of a specimen in the impact zone is reported in Figure 3. Finally the residual stresses due to the impact have been measured using an X-ray stress analyzer Stresstech Group v.1.01 model. Figure 4 show the average values of the residual stresses measured after the tests. The stresses, detected after the impact at a maximum distance of 20 mm from the hole tips, show in general two different trends, resulting predominantly of tensile type in the area adjacent to the entry zone of the projectile, and compressive in the exit zone.

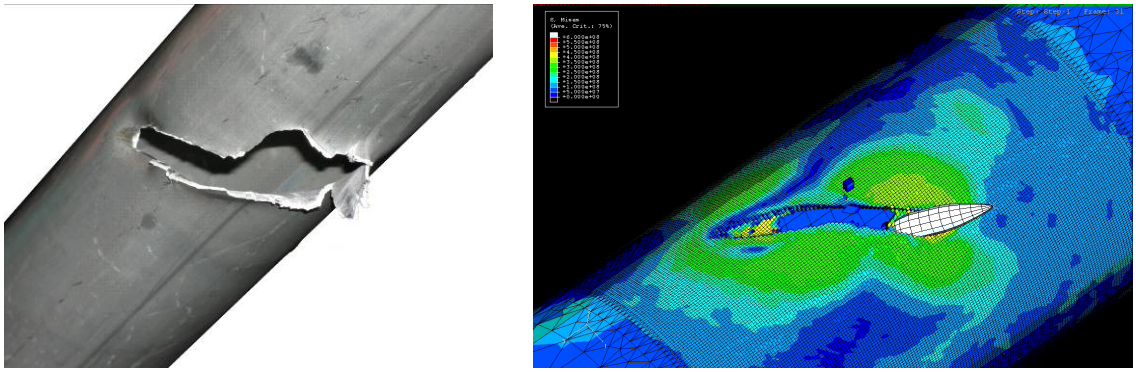

Figure 3 – Shape of the damage from experimental test and numerical simulation

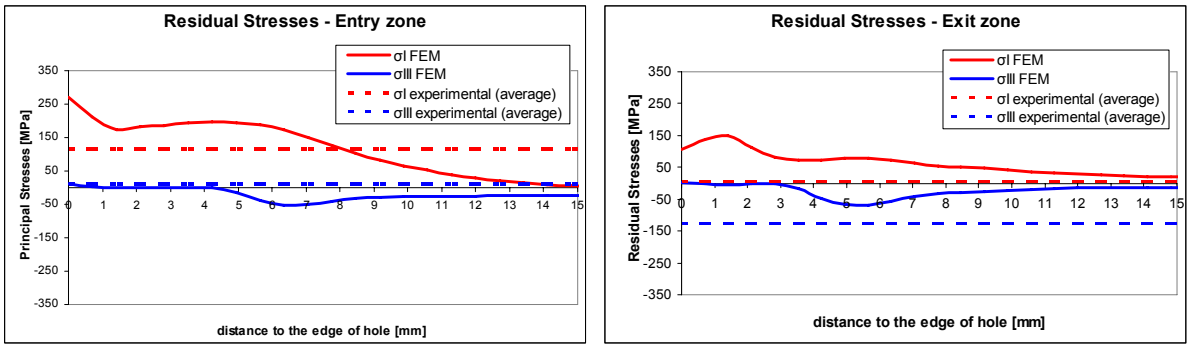

Figure 4 – Average value of residual stresses measured after the tests and from FEM

EXPERIMENTAL TORSIONAL TESTS

A fatigue torsional spectrum (Table 1), representing the operating load detected during a recovery mission at reduced power, has been applied on a damaged shaft with single

hole (worst case) using a hydraulic multiaxial test machine MTS 809 (Figure 5). During the first spectrum, a fatigue crack arises at the exit edge of the hole, and propagates in stable mode perpendicular to the maximum principal stress direction following a mainly mode I of propagation independent on the starting direction (Figure 5) as also reported in literature in similar tests [18,19]. However, as the numerical analyses have shown, due to the impact source of the damage, propagation does not follow just the mode I. The propagation has also been monitored by means of a Leica DFC290 optical microscope, equipped with hardware and software for image acquisition in order to measure the position of the crack tip (Fig. 5). The crack stops at the end of the first spectrum, and its final length is about 2.87 mm (Figure 6).

Table 1 – Applied load spectra

Spectrum	Minimum Torque [Nm]	Maximum Torque [Nm]	Cycles	R
1	160	256	2200	0.63
2	10	66	4200	0.15
3	6	54	160000	0.11

Figure 5 – Experimental set-up of the torsional tests

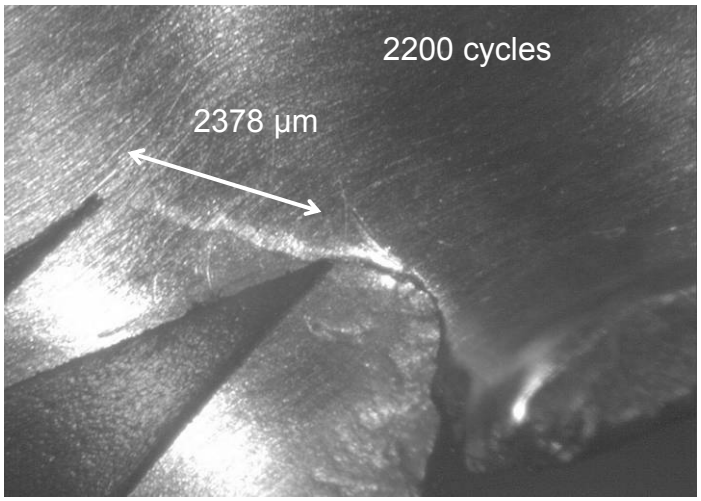

Figure 6 – The acquisition of the crack propagation with the Leica DFC290 optical microscope

NUMERICAL SIMULATION OF BALLISTIC IMPACT

Numerical analyses have been conduced using the commercial finite element code Abaqus Explicit v.6.7. The simulated impact conditions are the same of the experimental tests. The shaft has been modelled using 293,132 solid elements. The mesh has been divided in three areas, with increasing density.

The projectile is modelled as a rigid body; this is due to the lack of material characterization for high strain rate. Shaft material behaviour, for how concern strain rate, has been modelled using a Johnson-Cook [20] constitutive relation calibrated with

data from literature [21]. Johnson-Cook JC ductile failure criterion has also been used. The friction between the shaft and projectile surface has been neglected and no external loads are applied on the model. The applied condition of constraint prevents all translations of the nodes in one extreme, leaving free on the other end the translation along the tube axis. The principal model results are reported in Table 2; in Figure 3 is reported a "frame" of the FE model analysis of the shaft during the impact simulation.

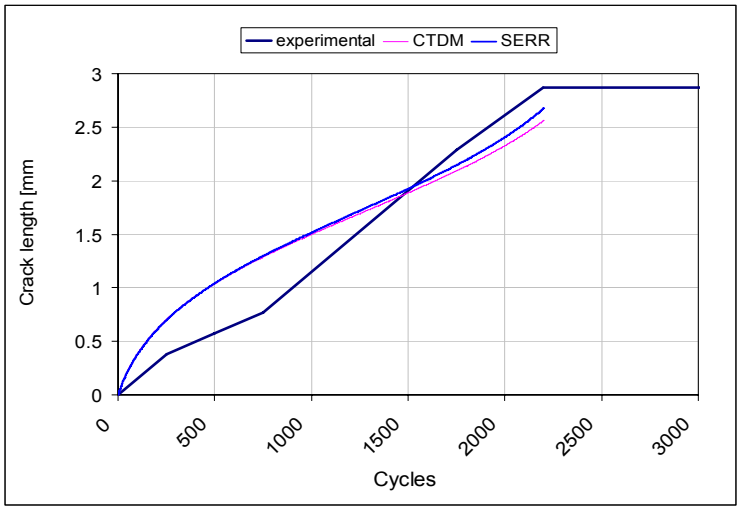

Figure 7 – Experimental data and numerical prediction of crack length (Crack Tip Displacement Model (CTDM) and Strain Energy Release Rate (SERR) approaches)

Table 2 – Experimental and numerical results ($^{(*)}$ average values of tests)

Parameter		Experimental	FE
V_i [m/s]	Initial velocity of projectile	850	851$^{(*)}$
V_R [m/s]	Residual velocity of projectile	819	744$^{(*)}$
l [mm]	Hole total lenght	70.5	75.8$^{(*)}$

NUMERICAL SIMULATION OF APPLIED LOAD SPECTRA

After the simulation of the impact, in order to simulate the further propagation stage, the perimeter of the damage has been manually elaborated. According to the fact that 4 elements have been placed along the thickness of the shaft in the impact zone, a rule of elimination has been set: if there are one of more elements erased during the simulation on the edge of the damage, all the elements, along the thickness in the same point, have been erased. This is functional for the next step in which a procedure for the evaluation of the most likely point of crack nucleation along the edge of the damage is performed. A dedicated program has been used to elaborate the input file of FE software (ABAQUS). Almost 140 analyses have been executed inserting a crack in different

points along the edge of the damage (a crack for each analysis) and the stress intensity factor K_I in each point has been calculated. In order to obtain reliable results a sub model has been analysed for each simulation (starting from the results obtained from the global model). The sub model is a cylinder with the crack starting from the longitudinal axle and with a dedicated focused mesh (quarter point). The analyses have been executed both considering the residual stresses from the previous impact analysis, Figure 4, and neglecting their effect. The results are reported in Figure 8, plotted starting from the entry point of the bullet. The entry and exit points are the most likely positions for the nucleation of fatigue cracks. Thus, according to the experimental observations, the crack propagation has been numerically studied starting from the exit point of the projectile. The crack propagation have been simulated using the same framework above explained, with crack positioned also in a global model and fracture mechanics parameters (SIF) obtained by the cylindrical submodel centred in the crack tip.

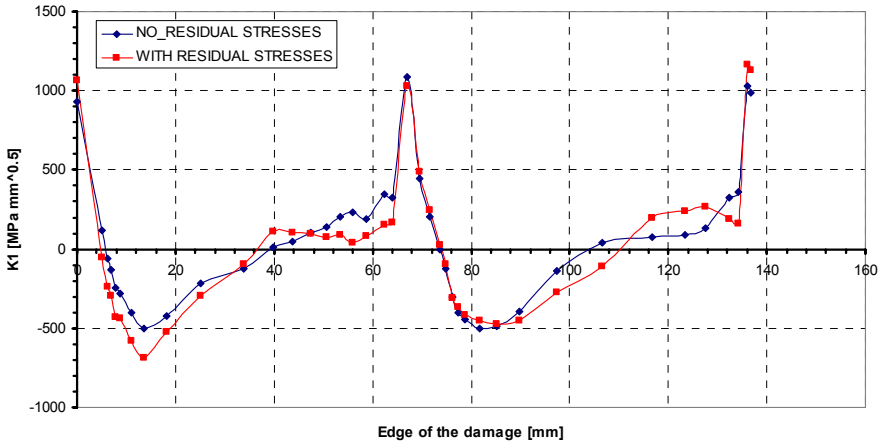

Figure 8 – Research of the most likely point for the crack nucleation with and without the effect of residual stresses.

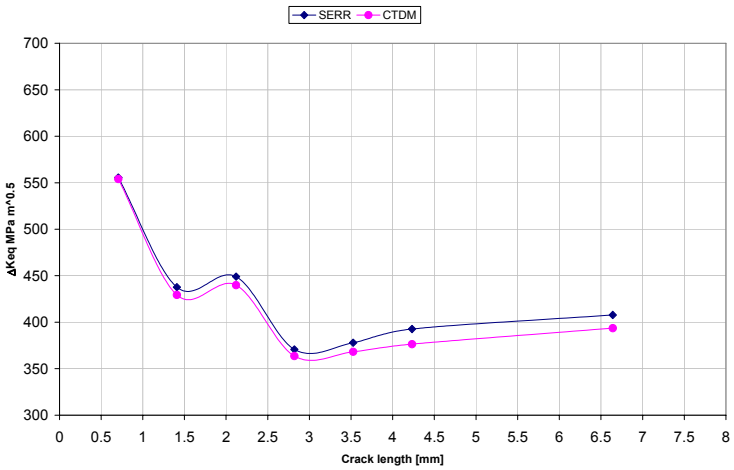

Figure 9 - Correlation of the ΔK_{eq} with crack length

The simulated crack propagated perpendicular to the principal nominal stress direction with discrete steps and the SIFs K_I, K_{II} and K_{III} have been acquired at each step. Only the loads of the spectrum 1 (Table 1) have been considered for the propagation; the loads of the other spectra are in fact lower than the propagation threshold value. Considering the residual stress field due to ballistic impact, two analyses have been performed at each step, respectively with the maximum (C_{max}) and minimum (C_{min}) torque of the spectrum 1. The value of the SIFs is the average of the stable value (stable is referred to the stabilization of the value obtained from different contours) along the thickness of the submodel and thus the $\Delta K_{I,II,III}$ are obtained, at each step, from the difference of the values obtained from the analysis with maximum and minimum torque. The analyses have been carried out from a starting crack of 0.7 mm until a final length of about 7 mm. Once the SIFs have been obtained for the whole extension of the crack, the next step is to simulate numerically the propagation. According to the mixed mode loading, the crack growth rate can be expressed by the Paris law where the classical Stress Intensity Factor range is expressed by an equivalent value (ΔK_{eq}). Different approaches have been proposed for how concern the mixed mode crack propagation for long cracks. Two formulations have been used in this work [22]: an approach based on the Crack Tip Displacement Model (CTDM, based on the work of Tanaka) and another based on Strain Energy Release Rate (SERR, based on the work of Irwin). Both the approaches combine the $\Delta K_{I,II,III}$ in order to obtain a single value of ΔK_{eq} applicable into a propagation law. Using a single parameter to describe the crack propagation behaviour is a direct assumption of the LEFM theory. The ΔK_{eq} resulting from each approach are reported in Figure 9. The results show a very little difference between the considered methods. On the contrary the presence of residual stresses leads to a not monotone increment. A good numerical estimation of the residual stress field is a key task in order to asses a reasonable propagation procedure [23] considering that the projectile exit zone (where the crack propagate) is characterized by a multiaxial state of stress due to compressive residual stresses and complex shape of the damage. During the experimental test, the observed crack is exactly perpendicular to the nominal maximum principal stress and parallel to the nominal minimum principal stress, and thus propagates along a spiral direction (Figure 6); this is the path also obtained in the numerical simulation. Therefore, the effect of transverse stress is small and the Mode I crack growth rate is the dominant one, with a Mode II contribution nearly reduced to zero. However, due to the shape and extension of the damage, during the torsional cycles there is a not planar separation of the crack surface that leads to a not negligible Mode III contribution in the propagation. Based on data represented in Figure 8, the crack propagation has been analytically evaluated using NASGRO relationship [24], expressed in (1), with material data furnished by the software itself (Table 3).

Table 3 – NASGRO parameters for AL 6061 T6

Material	σ_{YS} [MPa]	K_{Ie} [MPa√mm]	K_{Ic} [MPa√mm]	A_k	B_k	a_0 [mm]	C	n	p	q	ΔK_I [MPa√mm]	C_{th+}	C_{th-}	α
Al6061 T6	283	1251	938.2	1	0.75	0.0381	5.079E-10	2.3	0.5	0.5	45.52	1.50	0.1	2.0

$$\frac{dc}{dN} = C\left(\left(\frac{1-f}{1-R}\right)\Delta K_{eq}\right)^{n} \frac{\left(1-\frac{\Delta K_{th}}{\Delta K}\right)^{p}}{\left(1-\frac{K_{max}}{K_{C}}\right)^{q}} \quad (1)$$

DISCUSSION AND CONCLUSIONS

The comparison of the crack propagation data obtained from the experimental test and the numerical FE-NASGRO simulation shows that the experimental one (Figure 7) is a bit faster. In the same applied cycles the experimental crack length reaches 2.8 mm while with the numerical simulation with both the mixed mode models a crack length of 2.6 mm is obtained. Similar behaviour has been obtained in [18] with a similar but not equal loading case (defect from hole in tubular specimens under axial and torsional cyclic loading). It is important to state that the propagation model of this work is obtained by a previous critical impact analysis that lead to a complex multiaxial state of stress in the area interested for the crack propagation. Thus the accuracy of the propagation data is related also to the first stage of simulation; considering the complexity of the whole procedure the results achieved are considered very encouraging.

REFERENCES

1. Colombo D. *PhD. Thesis* , Politecnico di Milano, 2005.
2. Forrestal M. J., Piekutowsky A. J.. *Int. J. Impact Engng,* 1999.
3. Piekutowsky A. J., Forrestal M. J., Poormon K. L., Warren T. L. *Int. J. Impact Engng, 1999.*
4. Warren T. L., Poormon K. L.. *Int. J. Impact Eng,* 2001.
5. Roisman I. V., Weber K., Yarin A. L., Hohler V, Rubin M. B.. *Int. J. Impact Engng,* 1999.
6. Dey S., Børvik T., Hopperstad O. S., Leinum J. R., Langseth M.. *Int. J. Impact Engng*, 2004.
7. Børvik T., Hopperstad O. S., Langseth M., Malo K. A. *Int. J. Impact Engng*, 2002.
8. Børvik T., Langseth M., Hopperstad O. S., Malo K. A . *Int. J. Impact Engng*, 2000.
9. Børvik T., Langseth M., Hopperstad O. S., Malo K. A.. *Int. J. Impact Engng,* 1999.
10. Gupta N. K., Iqbal M. A., Sekhon G. S. *Int. J. Impact Engng*, 2005.
11. Zeinoddini M., Parke G. A. R., Harding J. E. *Int. J. Impact Engng*, 2000.
12. Gupta N. K., Madhu V. *Int. J. Impact Engng*, 1997.
13. Kezhun L., Goldsmith W. *Int. J. Impact Engng*, 1995.
14. Ning J., Song W., Wang J. *Acta Mech. Sinica*, 2005.
15. Hazell P.J., Edwards M.R., Longstaff H., Erskine J.. *Int. J. Impact Engng*, 36, 2009.
16. Bao Y., Wierzbicki T.. *International Journal of Mechanical Sciences*, 46, 2004.
17. Gilioli A.. *Master Science Thesis* , Politecnico di Milano, 2009.
18. Tanaka K., Takahash H., Akiniwa Y. *International Journal of Fatigue* 28 (2006) 324-334
19. Tcanov D., Sakane M., Itoh T., Hamada N. *International Journal of Fatigue* 30 (2008) 417-425
20. Børvik T., Dey S., Clausen A.H.. *Int. J. Impact Engng*, 36, 2009.
21. Lesuer D.R., Kay G.J., LeBlanc M.M. UCRL-JC-134118 2001
22. Socie D., Marquis G .“Multiaxial Fatigue” SAE 2000 ISBN 0-7680-0453-5
23. Pasta S., Reynolds A.P. *Fatigue Fract Engng. Mater Struct* 31, 569-580, 2008
24. NASGRO 4.11, Reference Manual, NASA Johnson Space Center, 2004.